ENGINEERING PLASMONIC NANOSTRUCTURES FOR FANO RESONANCE BASED BIOSENSOR

by
Yaozheng Li

A thesis submitted to Johns Hopkins University in conformity with the requirements for the degree of Master of Science

Baltimore, Maryland

May, 2017

ABSTRACT

Here we present a scheme and detailed theoretical investigation on the tunability of Fano resonance of gold nanodisks to utilize the unique feature of the plasmonic absorbance,which can potentially serve as imaging platforms. Gold nanodisk heptamer clusters have been shown to have a pronounced Fano resonance with specific dip regions. Here the heptamer has been separated into a ring structure and the central disk to analyze their hybridization effect, which contains the anti-bonding plasmonic mode and the bonding plasmonic mode. The trend of extinction spectra and electric field with modulation of structure and light propagation parameters shows a clear trend in the Fano resonance patterns. We have demonstrated the possibility of considerable tuning of the plasmonic lineshapes by altering the height of the disks, and also through tuning of parameters such as the refractive index of the substrate and by altering the direction of light propagation. The plasmon resonance lineshapes play a critical role in the tunable enhancement of plasmon-enhanced Raman scattering. The ability to tune the Fano lineshapes and the use of the nanopillar-like platforms as a scaffold for cellular growth makes it an important platform in multimodal imaging with an optimal budget of photon intensity thus reducing extensive cellular damage, photobleaching, and degradation.

Advisor: Ishan Barman

ACKNOWLEDGEMENT

This research is completed under the instruction of Prof. Ishan Barman and cooperated with Dr. Soumik Siddhanta.

The relative paper is under review.

TABLE OF CONTENTS

LIST OF FIGURES

INTRODUCTION

Biological research requires advanced approaches in imaging to analyze biological and chemical information. For this reason, a requirement of advanced imaging systems and tools would be inevitable. Various areas of works have been done to increase the performance of imaging and the quality of images. For instance, the contrast has been intensified by implementing phase contrast microscope; for more contrast in specific organelles inside the cell, fluorescent microscope has been developed and various kinds of dyes have been under research for improving the quality of the system. In other ways, the intensity of the signal for detection has been enhanced by surface plasmonic enhancements. One of the representation would be Surface Enhanced Raman Spectroscopy (SERS). Till now, a lot of researches are still concerning on image improving approaches. The combination of advanced optical tools and imaging modalities have made biological imaging more selective and effective while reaching ultra-high resolutions, even transcending the diffraction limit [1,2].

Among those enhancement methods, optical nanomaterials have always been selected as the source of surface plasmonic resonance. This kind of material has revolutionized several fields, especially in imaging. The excitation of localized surface plasmon resonance in nanostructured materials has been employed to study a variety of phenomena such as fluorescence enhancement, photonic upconversion and nearfield spectroscopic techniques [3-8]. What is more, this phenomenon can be coupled between nanomaterials to demonstrate the characteristic of the entire structure. For example, the formation of nanoparticle dimers and other forms of aggregates give rise to the intensity of the electromagnetic field which can be harnessed as hotspots. Based on this

combination effect of nanostructures, plasmonic hybridization can occur from the process and it can lead to effects like Fano resonances and electromagnetically induced transparency (EIT), which has a great potential in the development of imaging systems [9-11].

Fano Resonance is one of the most vital phenomena in noble metal nanostructures, it has attracted sufficient concentration from researchers in the field of biomedical imaging by its ability in generating EIT phenomenon. This phenomenon is desirable because it makes researchers capable of operating the process of imaging under a designated wavelength range [10]. The characteristic of Fano resonance is its asymmetric lineshape and researchers have found out discovered that this formulation is related to the formulas regarding Mie Theory [12]. To state that in detail, it is generated from the coupling acting between bonding and anti-bonding plasmonic modes between units inside of the nanostructure [13-27]. For all nanostructures which have been under research and experiment, the resource of the phenomenon would always be explained as above by separating the whole structure into groups or into asymmetric distribution. For instance, several symmetry-breaking structures can enable certain geometries such as cavities and concentric rings to display the characteristic of Fano line shape. As for some symmetrically distributed structures, they can also display the characteristic of Fano resonance which can be explained by group theory [28-34]. Another advantage of Fano resonance is that it can be tuned by adjusting structures to meet certain absorbance criteria, which can be harnessed for several optical applications [27,28]. According to particular extinction spectra, Fano dip can be discovered from the line shape and it would be possible for induce EIT phenomenon on the wavelength of the Fano dip so that it

would enable imaging to be more specific on certain chemical or biological substance by adjusting nanostructures. Moreover, the absorbance spectra of the structure would also lead to the specific enhancement for fluorophore because it would absorb more energy on the peak of the absorbance spectra so that less excitation light would be required for the same intensity of the fluorescence.

Excited by those potential applications and benefits it would provide with, there has been an increasing interest in structures exhibiting Fano resonance, represented by cubic structures with different distributions, nanoparticle and nanodisk with removed wedge and nanorods, etc [27,35-39]. As for heptamer arrangement of nanoparticles and nanodiscs, they have also between under research and they have been utilized as models in various optical studies.

Having relevance to surface plasmon resonance and Fano resonance, the localized surface plasmon resonance (LSPR) can lead to a stronger scattering and absorption several magnitudes more intense than the incident radiation. This phenomenon is of great usage on spectroscopy, imaging, and labeling, etc [13-15]. Combined with Fano resonance, various approaches ways of controlling the overall optical properties have been applied such as tune the interactions between adjacent nanostructure and the environment, basing on the fact that these are the two vital factors that influence the plasmonic properties, to acquire wider advancements in the areas of imaging and optics. The LSPR properties of plasmonic materials have been widely studies in the literature, but a gap in understanding about the coupling of various dipolar as well as multipolar plasmon resonance modes which would be critical for Fano Resonance. The link between Fano resonance and plasmonic resonances enables spectra with two distinct areas of

maxima separated by a Fano dip. The pronounced Fano dip helps in aligning the superradiant mode to the excitation as well as emission wavelengths in the case of fluorescence enhancement thus resulting in superior quantum yield [17]. In the case of fluorescence upconversion tool, this precise alignment of plasmonic modes to the laser excitation and emission results in enhancement, and the incident laser intensity can be reduced accordingly. This will greatly help in preventing biological systems such as cells and reporter molecules from photoinduced degradation and photobleaching.

As a result, in this thesis, we present a detailed investigation on the effect of structural parameters such as height combined to be heptamer structures and the role of the refractive index of the substrate on the line shape through discrete dipole approximation (DDA) calculations. The effect of forward and backward direction of light propagation as well as the effect of different angles of incidences on the heptamer have also been demonstrated. For the effect of height in electric field and Fano resonance, silver nanostructures would also be calculated for proving the reliability of the trend discovered in the gold structure because both of them are plasmonic metamaterials.

METHOD

The whole structure of plasmonic materials would be designed to be nanodiscs in heptamer configuration for the calculation of extinction spectra and electric field intensity distribution. Three sets of the structures would be utilized. One with no substrate below the nanodiscs and the other two with glass substrate and AlGaSb substrate, respectively. The schematics of the models are displayed in Figure 1. The diameter of the discs without substrate was fixed at 130 nm and the height of the nanodiscs was varied from 30 to 80 nm with the interval of 80 nm. As for the sets with substrates, the height is fixed at the value of 30 nm. For this simulation, the surrounding medium was air and the spectra were calculated from the wavelength between 400 nm and 1000 nm. As for the electric field simulation, the wavelength would be chosen on the point of the Fano Dip occurs. Then the characteristics of the spectra would be discussed.

The calculation method was performed by using Discrete Dipole Approximation method, which is considered to be one of the most efficient approaches in the field of plasmonic nanoparticle calculations. This approach can obtain exact solutions for the scattering of radiation of particles with greater accuracy. More details of DDA method are described elsewhere [19-21]. DDA method requires the division of dipoles. In these simulations, the dipole size was set at 5 nm. The DDA calculations were performed through DDSCAT 7.3.0 code developed by Draine and Flatau [19-21].

Similar calculations utilizing DDA method would also be operated on the silver structure with no substrate for the spectra and electric field intensity. The structure would be arranged in the same heptamer pattern and same geometry for a comparison of the result with that of the gold nanostructure.

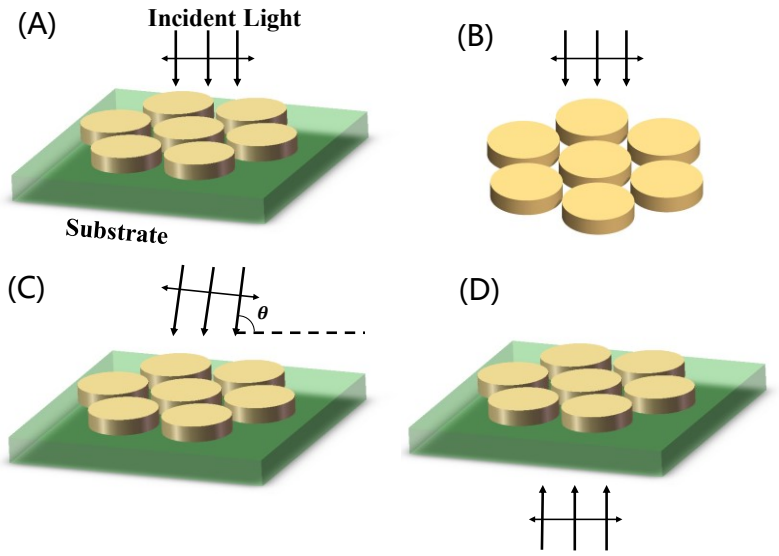

Figure 1 Schematic of nanostructures to be calculated (A-D) Schematic showing the gold heptamer structures in different substrate configurations and direction of incident light.

For the extinction spectra, it is measured by the value of extinction coefficient, which can be described by $Q_{ext} = \sigma_{ext}/\pi r_{eff}^2$, where r_{eff} represents the effective radius of the whole model. If the volume of the whole model is determined as V, then the effective radius is $r_{eff} = (3V/4\pi)^{1/3}$. The DDSCAT code was used to calculate the extinction spectra and the electric field distribution around the nanostructures [ref]. As for the electric field, DDSCAT can also put out a solution by operating through the nearfield mode.

The dipolar charges were calculated using Finite Difference Time Domain method by Lumerical FDTD (Lumerical Inc.) and the coupling or hybridization was determined among different dipolar or higher order modes and hence analyze the relation between

Fano lineshapes and hybridization modes. By calculating through the method mentioned above, the results and discussions can be demonstrated as below.

RESULTS AND DISCUSSIONS

Geometry of the gold nanodisks and Fano Resonance

The schematic of the plasmonic system without substrate is displayed in Figure 1 (a). DDSCAT code with DDA method was utilized to calculate the scattering spectra, absorption spectra and thus, get the extinction spectra because extinction spectra are the superposition of the scattering and absorption spectra. Meanwhile, the near-field distribution of the gold nanodisk clusters would be finished. Fano resonance effect was observed and extensively reported in the literature [23]. This resonance effect arises from the interference between the bonding on the bright mode and the anti-bonding on the dark mode. The dip in the extinction spectrum of the Fano dip is highly sensitive to the environment and the geometry. The geometry is responsible due to the fact that in the bonding mode, the dipolar plasmons of all disks are in the same phase and oscillate together. Conversely, in the anti-bonding mode, the dipolar moment of the central particle of the heptamer has opposite dipole to that of the outer ring [24]. The interference between these two modes results in Fano dip which can be tuned to different wavelengths by varying the disks [25]. The disks chosen as our model has a diameter and separation of 130 nm and 15 nm, respectively. The angle of polarization was kept constant in our studies as the optical properties of this heptamer with a D_{6h} symmetry makes it independent of the in-plane polarization of the incident light. The changes in diameter of the disks and distances have been known to alter the Fano line-shapes, the parameters such as the influence of the underlying substrate as well as the height of the disk, two of the parameters that can be controlled through electron beam or other lithographic processes has been unexplored so far, and has been presented in the following sections.

Dependence of Fano lineshape on disk height

From the extinction spectra shown in Figure 2 for gold structure, it was evident that the Fano lineshapes were dependent upon the height of the nanodisks in the heptamer nanostructure. These changes in Fano lineshapes can be explained by a simplified model of bonding mode and anti-bonding mode between the ring structure consisting of six disks and the central disk of the heptamer [10]. The scheme has been utilized to demonstrate the combination effect of the two modes because of the changes and shifts in the Fano resonant lineshapes and its dependence on the height of the disks.

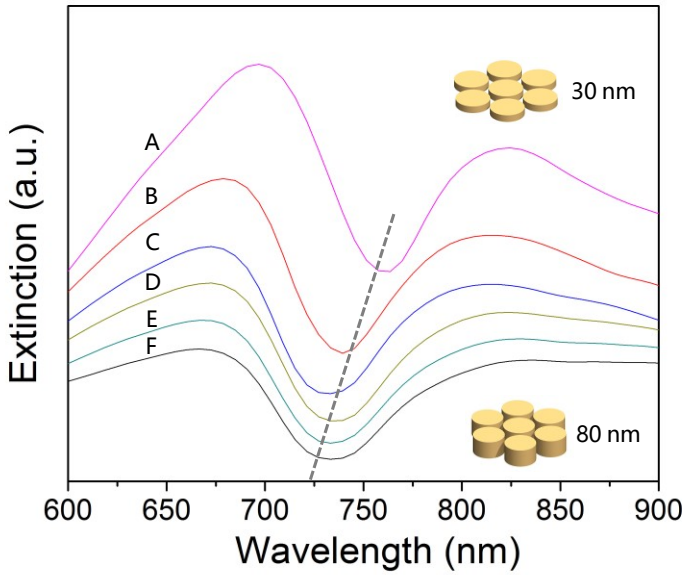

Figure 2 Extinction spectra after calculation for gold nanostructure without substrate (A-F) The extinction spectra of heights 30, 40, 50, 60, 70 and 80 nm gold nanodisks respectively, in heptamer configuration.

From the extinction spectra of gold and silver nanocluster, it is obvious that with the increasing value of height, the peak value decreases and also blue shifts. The same action

would be observed from the Fano dip. For gold nanostructure, the peak at 700 nm shifts to 650 nm and the dip shifts from 760 nm to 725 nm with the height increases from 30 nm to 80 nm. This blue shift is the result of the weaker hybridization of the higher modes as described below.

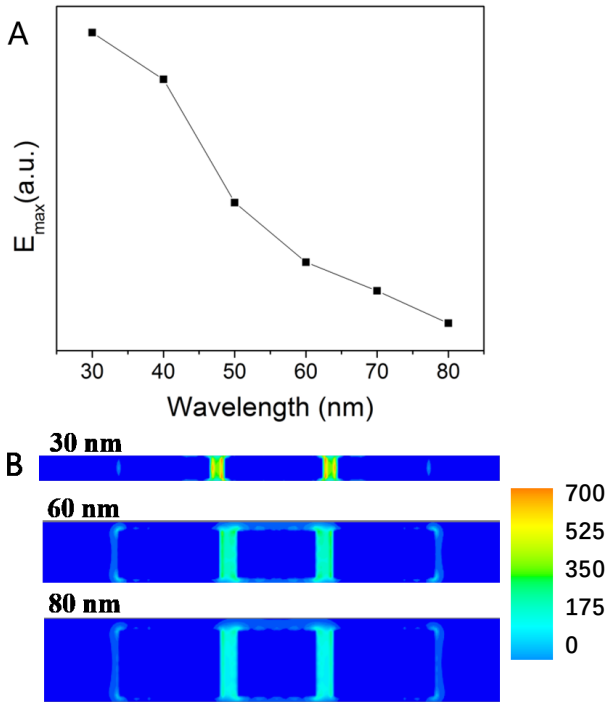

Figure 3 Electric field intensity result for gold nanostructure without substrate (A) Maximum electric field intensity around the gold nanodisk heptamer of different heights. (B) The electric field distribution around the gold nanodisks of different heights.

Not only does the Fano lineshape changes in terms of frequency shifts, but also in terms of electric field intensity distribution around the nanodiscs which is shown in Figure 3. The electric field drops from a height of 30 nm to 80 nm. The decrease in electric field intensity with increasing height of the nanodiscs is due to the retardation effect, observed when the disks sizes are increased along with a change in hybridization as discussed later. The electric field intensities were calculated at the wavelength of the

Fano dip so that the lowest extinction coefficient can be considered. The electric field contour and trend of maximum values are demonstrated in Figure 3.

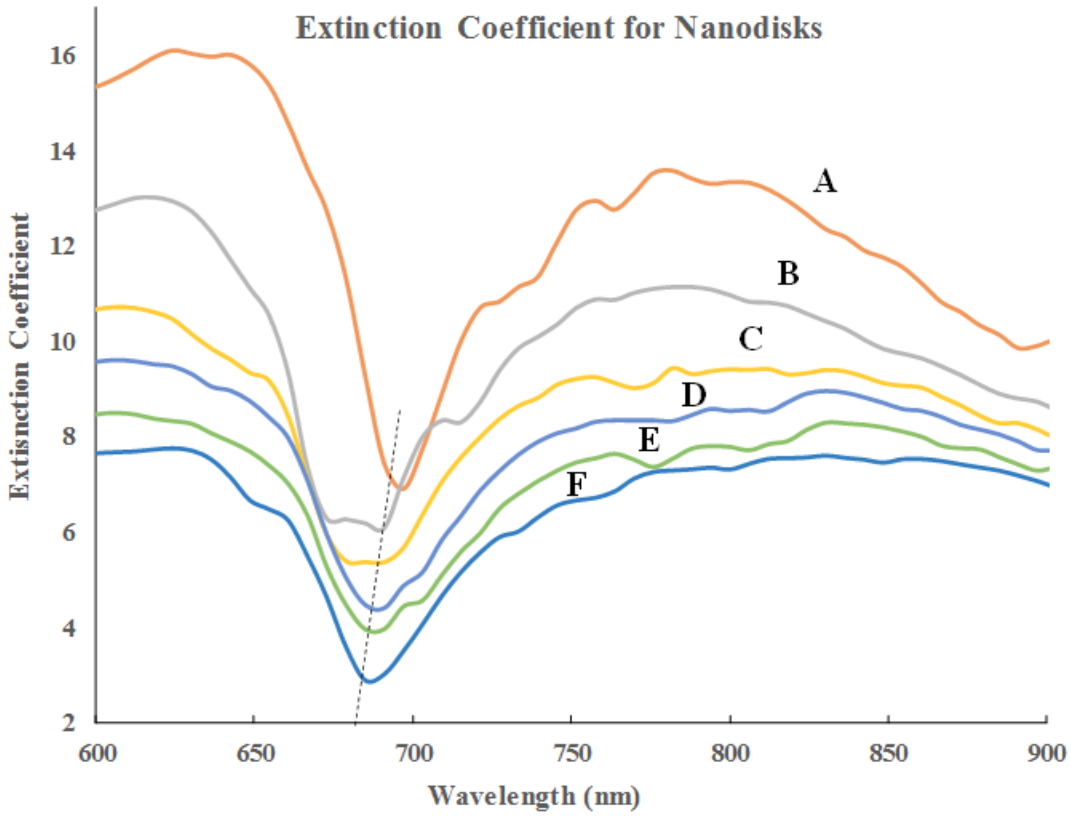

Figure 4 Extinction spectra after calculation for silver nanostructure without substrate (A-F) The extinction spectra of heights 30, 40, 50, 60, 70 and 80 nm gold nanodisks respectively, in heptamer configuration.

As for the circumstance of silver nanodisk heptamer, it would have similar trends of the extinction spectra showing the Fano resonance with Fano dip blue shifting and so as the bonding peak. The spectra of the silver structure have been illustrated in Figure 4. The difference from the gold nanostructure spectra is that the shift of the Fano dip and the

peak is lower than that of gold ones, which shifts from 700 nm to 680 nm for the Fano dip and 650 nm to 630 nm for the peak of bonding mode.

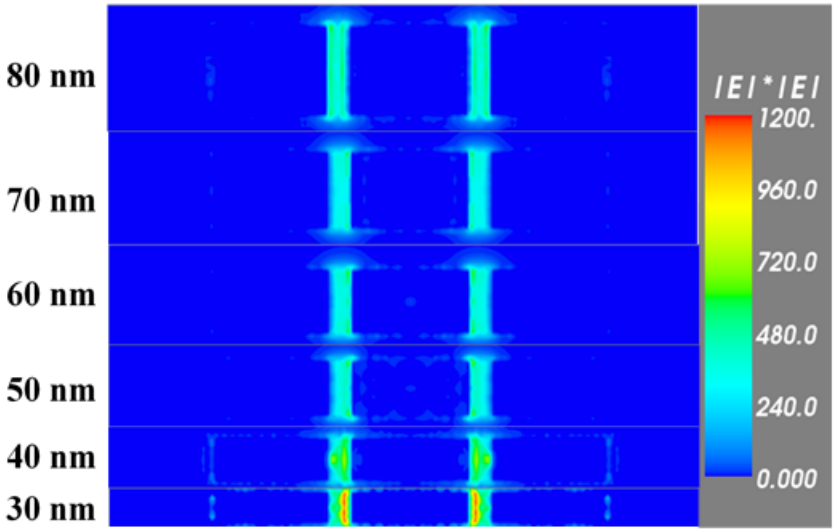

Figure 5 Electric field intensity result for gold nanostructure without substrate. The electric field distribution around the gold nanodisks of different heights.

In addition, for the electric field intensity of the whole structure in silver, electric field contours have been demonstrated. Although a curve demonstrating the trend of the maximum electric field intensity is absent for the silver structure, it is still obvious that the electric field intensity is dropping with the increasing height of those nanodiscs. From all those results displayed from the silver nanostructure, it can be proven that the outcome of gold nanostructure would be reliable and valuable for further explanation for harnessing.

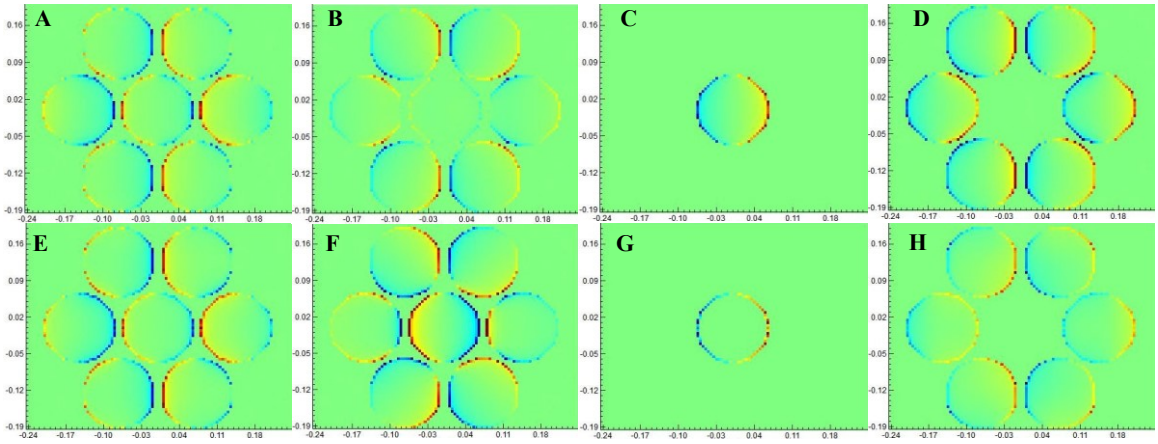

Figure 6 Charge distribution for nanostructures without substrate (A), (B), (C), (D) represents charge distribution of the bonding mode, anti-bonding mode, single nanodisk and ring structure with the height of 30 nm, respectively; (E), (F), (G), (H) represents charge distribution of the bonding mode, anti-bonding mode, single nanodisk and ring structure with the height of 60 nm, respectively.

To explain this phenomenon, it can be explained in detail by schematics of plasmonic hybridization by claiming the vibration direction of charges inside the nanostructure. It is known that Fano resonance is generated from the hybridization of two plasmonic modes and the deeper the Fano dip, the stronger the resonance would be. To assign different modes in the extinction spectra, the charge distribution modes in heptamer nanodisks with the height of 30 nm has been calculated through Lumerical FDTD and the result is shown in Figure 6 (A-D). For the structure with the height of 60 nm, the charge distribution result is provided in Figure 6 (E-H). Based on the distribution of the positive and negative charges, the directions of the dipoles could be displayed as shown in the scheme in Figure 5. Conventionally, the arrows follow a direction from positive to negative charge. The charge distribution plots show the origin of Fano resonance with the superradiant and subradiant charge plots showing dipolar and multipolar components respectively. The bonding and the antibonding modes are shown

in Figure 7 (A-C). The direction of dipoles is in the same direction in the bonding mode. On the other hand, when the wavelength comes to the value of the Fano dip position, it comes to an anti-bonding mode, leading to a mixture of quadrupolar modes among the nanodiscs. In order to prove that the bonding and anti-bonding mode are generated from the interaction between structures and explain the resultant Fano effect, two different groups of disks: a ring without the central disk and the central disk itself was used to show the plasmonic coupling. They would not have quadrupolar modes if they are calculated alone as shown in the left and right side of the scheme with a single direction of the dipole, representing that the combined effect can lead to the multipolar modes. For the bonding mode between those groups, the dipolar moments are in phase resulting in enhanced radiative damping and broadening of the modes. However, as for the anti-bonding mode, the dipolar moments between those two groups would be out of phase with the dipoles of disks opposing each other. Thus, the total dipole moment tends to be almost zero, leading to a sharp dip in the spectra.

For two different disk heights of 30 nm and 60 nm, the dipolar coupling was lower in the case of 60 nm disks because of the higher damping and lower resonance induced by the larger size, leading to a flatter spectrum for both the single disk and the ring structure for the disks with larger heights. The wavelength of those peaks and dips in the absorption spectrum can be explained by the energy of the incident light. When the height is relatively low in value, the energy required for oscillation would be less because of the lower damping energy to overcome for the generation of oscillating dipoles and vice-versa, when the height is more. Therefore, there is a red-shift of both the sub and superradiant modes in the case of the higher height of the disks. The increase in height

also results in the decrease of electric field intensity around the disks. With the damping of the dipolar modes, the surface plasmon resonance will also be affected resulting in the decrease in the electric field with height.

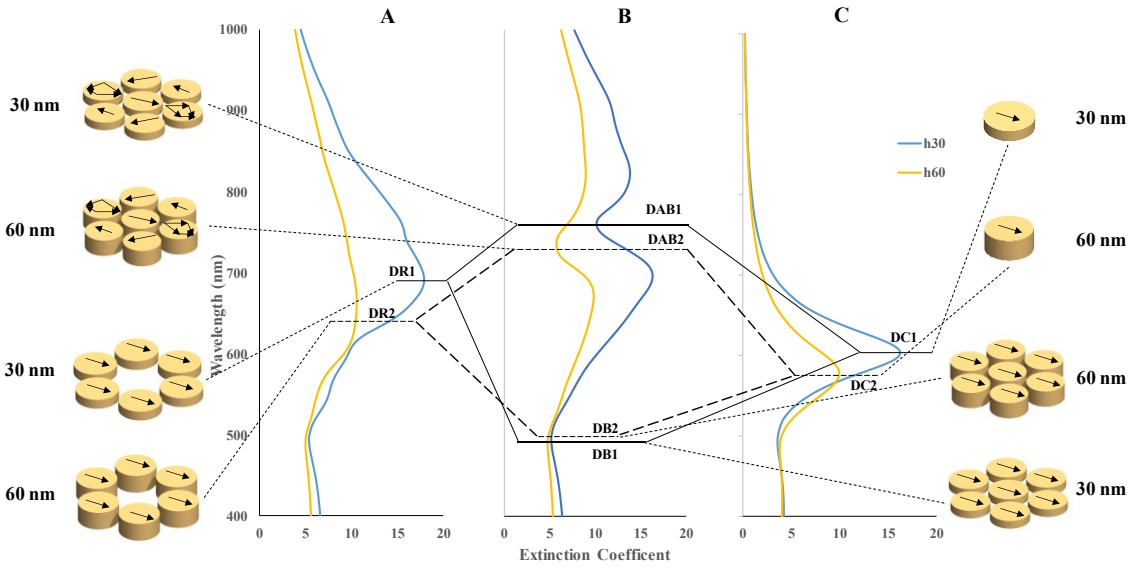

Figure 7 Schematic of nanostructure hybridization Schematic describing the hybridization of different gold nanodisks conformations with different heights. (A), (B) and (C) corresponds to the spectra of nanodisk rings, the spectra of the heptamer, the spectra of a single nanodisk, respectively.

Dependence of Fano resonance and nearfield intensity on substrate refractive index

The effect of dielectric substrate on the gold nanodisk heptamer has been investigated. The introduction of a layer of glass with a thickness of 200 nm as a support for the heptamer induces a shift in the Fano dip as well as superradiant modes which are shown in Figure 8. There is a shift of around 50 nm of the superradiant mode and 50 nm of the Fano dip. The intensity of the overall extinction coefficient also decreases as compared to the situation when the underlying substrate is absent. The electromagnetic

field distribution around the gold disks is shown in Figure 9. The decrease in the scattering and extinction in using higher refractive index substrate such as glass (n=1.5) led us to investigate the extinction for even higher refractive index substrate such as AlGaSb with a refractive index of 4.6. In this case, we observe a higher scattering background but much reduced intensity of the superradiant modes as well as the Fano dip. The multipolar modes have broadened and shifted to higher wavelengths when compared to that of without substrate. The high refractive substrates are known to lower the symmetry of the system and allow the mixing of dipolar and multipolar modes [32]. The substrate itself results in enhanced scattering and its intensity is more than absorption in the extinction spectra. The intensity of Fano dip was also significantly reduced. Therefore, for imaging as well as enhancement techniques such as SERS, a substrate with a lower refractive index is preferred. Whereas in the case of photothermal applications, the use of higher refractive index materials as substrates is more essential. Also, in order to tune the extinction maximum to higher wavelengths, the tuning of refractive index to higher values is necessary.

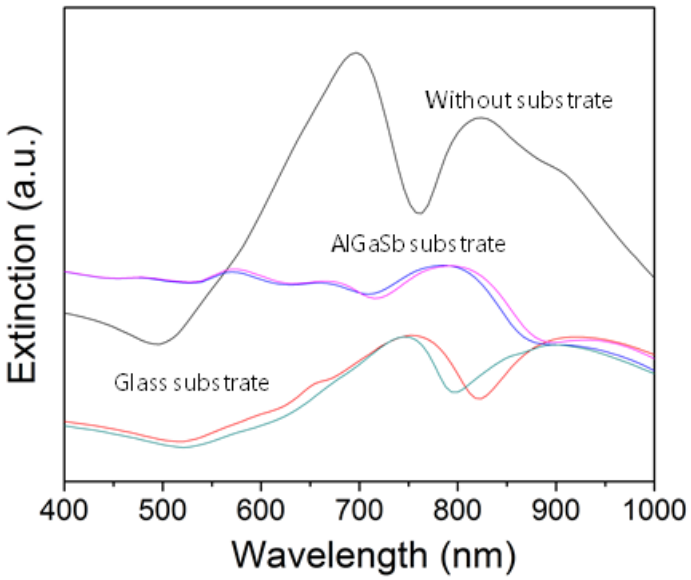

Figure 8 Extinction spectra for substrate comparison Extinction spectra of gold nanodisk heptamers on different substrates and at different directions of light propagation (front and back).

Dependence of Fano lineshapes on direction of light propagation

The direction of light propagation, incident normally either from the substrate side or the heptamer side, has implications on the distribution of electromagnetic field around the nanodisks. In conventional settings, the exciting light generates surface plasmons of the nanoparticles and the resultant light passes through the underlying substrate. From Figure 9 it is evident that the when the light is incident on the hexamer first, the electromagnetic field intensity and distribution are almost similar in the case of glass. But in the case of AlGaSb, the difference between electromagnetic intensity between the front and back illumination is significantly higher. This is because the high refractive index substrate strongly absorbs the incident light and diminishes the light which excites the surface plasmons of the nanodisks. The line shape of the Fano resonance changes greatly

in case of higher refractive index substrate both when the light is incident on the disks or on the substrate first.

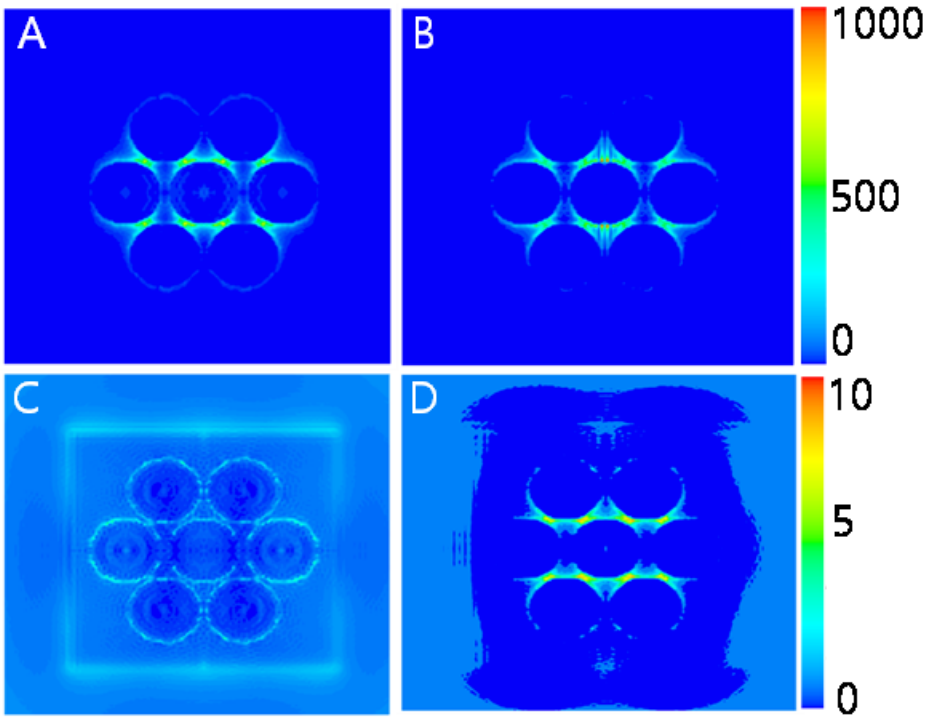

Figure 9 Electric field comparison on the refractive index of substrate Electric field distribution around the gold nanodisk heptamers on different substrates and directions of incident light. (A) and (B) corresponds to nanodisks on a glass substrate in forward and backward light directions respectively. (C) and (D) corresponds to nanodisks on AlGaSb substrate in forward and backward light directions respectively. The diameter of the nanodisk was 130 nm.

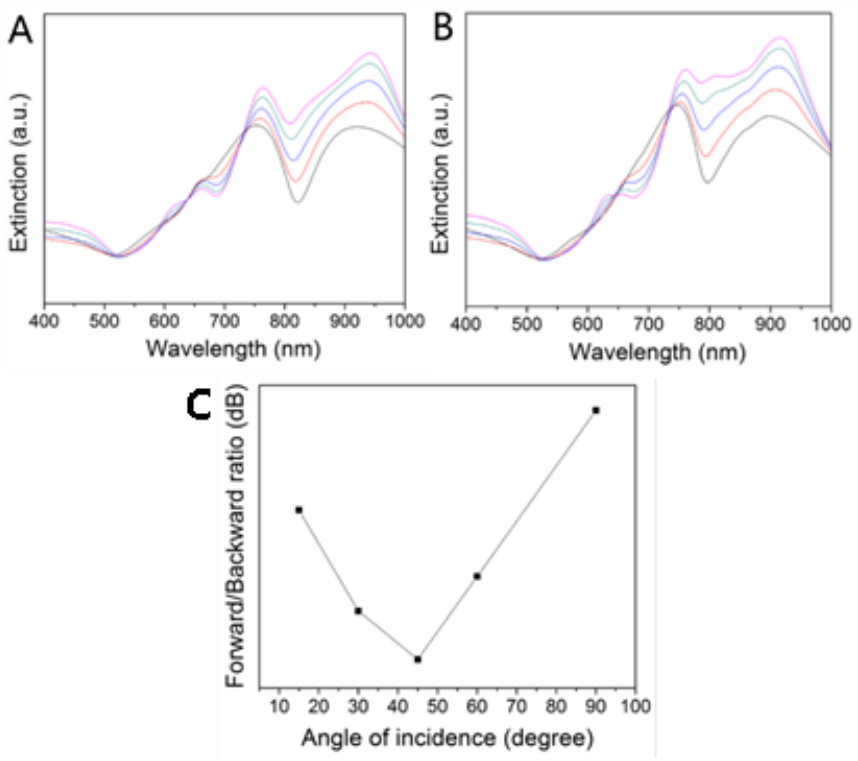

Figure 10 Comparison of extinction spectra with various incident light angle and directions The extinction spectra of gold nanodisk heptamer when the angle of incidence of light is changed from 15 to 90 degrees. Pink, green, blue, orange and black lines correspond to angles of 15, 30, 45, 60 and 90 degrees respectively. (A) and (B) corresponds to direction of light from the nanodisk face and from the substrate (glass) face respectively. (C) corresponds to the forward/backward ratio of the extinction coefficient with the incidence of light ranging from 15 to 90 degrees.

The change in incidence angle showed that normal incidence leads to the maximum Fano dip although the scattering intensity from the extinction spectra is lower as shown in Figure 10 (A) and Figure 10 (B). This is consistent with the fact that the change in direction of light also results in the change in angle of polarization of the incident light which has implication on the Fano lineshapes. Also, when the light is incident at an angle, the absorbance from the substrate also increases as the distance traversed is increased. The change in the Fano dip is observed much more intensely when the light is incident

from the glass side rather than the heptamer side. The forward to backward incidence ratio is shown in Figure 10 (C). Initially, from normal until 45 degrees of angle of incidence from the heptamer side, the electromagnetic field intensity decreases gradually. But at a much lower angle of incidence, the ratio starts increasing again. It is to be noted that the forward to backward ratio is much lesser than 1. That means the intensity from the front is always lesser than that of the back.

CONCLUSION

We have reported the structural parameters that are critical in controlling plasmonic Fano lineshapes. It was evident that the height and the underlying substrate play an important role in the intensity of the extinction as well as the position and depth of the Fano dip because of the adjustment in the hybridization between bonding mode and anti-bonding mode of the whole structure under different wavelength.

When it comes to the substrate, substrates with various refractive indices would lead to different effects on the response extinction spectra and electric field intensity. With a higher refractive index of the substrate, the scattering action would be intensified by the substrate and as a result, the whole spectra would be overwhelmed by this substrate, leading to a lower Fano dip. Considering electric field intensity, the substrate with a higher refractive index would lead to a lower difference between electromagnetic intensity between the front and back illumination would be significantly higher, leading to a selection of the direction of light in electric field.

Finally, for the direction of the illumination, i.e. the direction of the polarization of the light, the extinction spectra would also be affected, especially from the substrate side because of the scattering effect of the substrate. It would lead to the most intense Fano dip when it is vertical and gradually weakens.

By precisely controlling the height and the refractive index, coupled with the direction and angle of light propagation, it is possible to tune the position of Fano dip, the plasmonic nearfield intensity and the overall plasmonic enhancement in selective wavelength ranges and thus, this phenomenon can be harnessed to be implemented in a

higher efficiency fluorescence performance and also can be adjusted to some specific spectroscopy measurement when making usage of the Fano dip position.

REFERENCE

(1) Weissleder, R.; Ntziachristos, V. Nat. Med. 2003, 9, 123-128.

(2) Balas, C. Meas. Sci. Technol. 2009, 20 (10), 104020.

(3) Jain, P. K.; Huang, X.; El-Sayed, I. H.; El-Sayed, M. A. Acc. Chem. Res. 2008, 41 (12), 1578-1586.

(4) Ray, P. C. Chem. Rev. 2010, 110 (9), 5332-5365.

(5) Bardhan, R.; Grady, N. K.; Cole, J. R.; Joshi, A.; Halas, N. J. ACS Nano 2009, 3 (3), 744-752.

(6) Le, K. Q.; John, S. Opt. Express 2014, 22 (S1), A1-A12.

(7) Zayats, A. V.; Smolyaninov, I. J. Opt. A 2003, 5 (4), S16.

(8) Anker, J. N.; Hall, W. P.; Lyandres, O.; Shah, N. C.; Zhao, J.; Van Duyne, R. P. Nat. Mater. 2008, 7 (6), 442-453.

(9) Ghosh, S.K.; Pal, T. Chem. Rev. 2007, 107 (11), 4797-4862.

(10) Luk'yanchuk, B.; Zheludev, N. I.; Maier, S. A.; Halas, N. J.; Nordlander, P.; Giessen, H.; Chong, C. T. Nat. Mater. 2010, 9 (9), 707-715.

(11) Zhang, S.; Genov, D. A.; Wang, Y.; Liu, M.; Zhang, X. Phys. Rev. Lett. 2008, 101 (4), 047401.

(12) Lassiter, J. B.; Sobhani, H.; Knight, M. W.; Mielczarek, W. S.; Nordlander, P.; Halas, N. J. Nano Lett. 2012, 12 (2), 1058-1062.

(13) Rybin, M. V.; Samusev, K. B.; Sinev, I. S.; Semouchkin, G.; Semouchkina, E.; Kivshar, Y. S.; Limonov, M.F. Opt. Express 2013, 21 (24), 30107-30113.

(14) Rybin, M. V.; Filonov, D. S.; Belov, P. A.; Kivshar, Y. S.; Limonov, M. F. Sci. Rep. 2015, 5.

(15) Forestiere, C.; Negro, L. D.; Miano, G.; Phys. Rev. B 2013, 88 (10), 155411.

(16) Artar, A.; Yanik, A. A.; Altug, H. Nano Lett. 2011, 11 (4), 1685-1689.

(17) Giannini, V.; Francescato, Y.; Amrania, H.; Phillips, C. C.; Maier, S. A. Nano Lett. 2010, 10 (10), 2835-2840.

(18) Gallinet, B.; Martin, O. J. F.; Phys. Rev. B 2011, 83 (23), 235427.

(19) Pryce, I M.; Aydin, K.; Kelaita, Y. A.; Briggs, R. M.; Atwater, H. A.; Nano Lett. 2010, 10 (10), 4222-4227.

(20) Hao, F.; Norlander, P.; Sonnefraud, Y.; Van Dorpe, P.; Maier, S. A. ACS Nano 2009, 3 (3), 643-652.

(21) Woo, K. C.; Shao, L.; Chen, H.; Liang, Y.; Wang, J. F.; Lin, H. Q. ACS Nano 2011, 5 (7), 5976-5986.

(22) Chen, H. J.; Shao, L.; Ming, T.; Woo, K. C.; Man, Y. C.; Wang, J. F.; Lin, H. Q. ACS Nano 2011, 5 (7), 6754-6763.

(23) Zhou, W.; Odom, T. W.; Nat. Nanotechnol. 2011, 6 (7), 423-427.

(24) Liu, N.; Weiss, T.; Mesch, M.; Langguth, L.; Eigenthaler, U.; Hirscher, M.; Sonnichsen, C.; Giessen, H. Nano Lett. 2010, 10 (4), 1103-1107.

(25) Zhou Z. K.; Peng, X. N.; Yang, Z. J.; Zhang, Z. S.; Li, M.; Su, X. R. Zhang, Q.; Shan, X. Y.; Wang, Q. Q.; Zhang, Z. Y.; Zhang, Z. Y. Nano Lett. 2011, 11 (1), 49-55.

(26) Yanik, A. A.; Cetin, A. E.; Huang, M.; Artar, A.; Mousavi, S. H.; Khanikaev, A.; Connor, J. H.; Shvets, G.; Altug, H. Proc. Natl. Acad. Sci. U.S.A. 2011, 108 (29), 11784-11789.

(27) Lassiter, J. B.; Sobhani, H.; Fan, J. A.; Kundu, J.; Capasso, F.; Nordlander, P.; Halas, N. J. Nano Lett. 2010, 10 (8), 3184-3189.

(28) Hao, F.; Sonnefraud, Y.; Van Dorpe, P.; Maier, S. A.; Halas, N. J.; Nordlander, P. Nano Lett. 2008, 8 (11), 3983-3988.

(29) Mirin, N. A.; Bao, K.; Nordlander, P. ACS Nano 2009, 113 (16), 4028-4034.

(30) Sonnefraud, Y.; Verellen, N.; Sobhani, H.; Vandenbosch, G. A. E.; Moshchalkov, V. V.; Van Dorpe, P.; Nordlander, P.; Maier, S. A. ACS Nano, 2010, 4 (3), 1664-1670.

(31) Le, F.; Brandl, D. W.; Urzhumov, Y. A.; Wang, H.; Kundu, J.; Halas, N. J.; Aizpurua, J.; Nordlander, P. ACS Nano 2008, 2 (4), 707-718.

(32) Zhang, S.; Bao, K.; Halas, N. J.; Xu, H.; Nordlander, P. Nano Lett. 2011, 11 (4), 1657-1663.

(33) Fan, J. A.; Wu, C.; Bao, K.; Bao, J.; Bardhan, R.; Halas, N. J.; Manoharan, V. N.; Nordlander, P.; Shvets, G.; Capasso, F. Science 2010, 328 (5982), 1135-1138.

(34) Hentschel, M.; Saliba, M.; Vogelgesang, R.; Giessen, H.; Alivisatos, A. P.; Liu, N. Nano Lett. 2010, 10 (7), 2721-2726.

(35) Yang, Z.; Wang, M.; Song, X.; Deng, J.; Yao, X. J. Chem. Phys. 2013, 139 (16), 164713.

(36) Fang, Z.; Cai, J.; Yan, Z.; Nordlander, P.; Halas, N. J.; Zhu, X. Nano Lett. 2011, 11 (10), 4475-4479.

(37) Sivapalan, S. T.; DeVetter, B. M.; Yang, T. K.; Van Dijk, T.; Schulmerich, M. V.; Carney, P. S.; Bhargava, R.; Murphy, C. J. ACS Nano 2013, 7 (3), 2099-2105.

(38) Dregely, D.; Hentschel, M.; Giessen, H. ACS Nano 2011, 5 (10), 8202-8211.

(39) Ye, J.; Wen, F.; Sobhani, H.; Lassiter, J. B.; Van Dorpe, P.; Nordlander, P.; Halas, N. J. Nano Lett. 2012, 12 (3), 1660-1667.

(40) Zhao, J.; Zhang X.; Yonzon, C. R.; Haes, A. J.; Van Duyne, R. P. Nanomed. 2006, 1 (2), 219-228.

(41) Huang, X.; Jain, P. K.; El-Sayed, I. H.; El-Sayed, M. A. Lasers Med. Sci. 2008, 23 (3), 217.

(42) Roper, D. K.; Ahn, W.; Hoepfner, M. J. Phys. Chem. C 2007, 111 (9), 3636-3641.

(43) Liz-Marzán, L. M. Langmuir 2006, 22 (1), 32-41.

(44) Liu, S.; Huang, L.; Li, J.; Wang, C.; Li, Q.; Xu, H.; Guo, H.; Meng, Z.; Shi, Z.; Li, Z. J. Phys. Chem. C 2013, 117 (20), 10636-10642.

(45) Liu, X.; Lei, D. Sci. Rep. 2015, 5.

(46) Draine, B. T.; Flatau, P. J. J. Opt. Soc. Am. A 1994, 11 (4), 1491-1499.

(47) Flatau, P. J.; Draine, B. T. Opt. Express 2012, 20 (2), 1247-1252.

(48) Flatau, P. J.; Draine, B. T. Opt. Express 2014, 22 (18), 21834-21846.

(49) Hooshmand, N.; Panikkanvalappil, S. R.; El-Sayed, M. A. J. Phys. Chem. C 2016, 120 (37), 20896-20904.

CURRICULUM VIT

Yaozheng Li

500 W University Pkwy, Baltimore, MD 21210, USA

Tel: +1-(443)360-8783

Email: yli213@jhu.edu

EDUCATION AND TRAINING

09/2015-05/2017 Johns Hopkins University

Major: Mechanical Engineering

Degree: Master of Science in Mechanical Engineering

Specialty: Photonics for Quantitative Biology and Medicine

09/2011-06/2015 Wuhan University, China

Major: Mechanical Engineering

Degree: Bachelor of Engineering in Mechanical Engineering

Thesis: Research on the comfort of N95 filtering facial respirator (Advisor: Hui Li)

PROFESSIONAL EXPERIENCE

09/2015-05/2017 Graduate Research Assistant (Master Student)

09/2016-12/2016 Teaching Assistant (EN 530.473 Molecular Spectroscopy and Imaging)

RESEARCH EXPERIENCES

11/2016-05/2016 Fano analysis of nanorod waveguide upon nanodisk structures, Advisor: Ishan Barman, Johns Hopkins University

- Calculated the extinction spectra of nanodisk structure with a gold nanorod waveguide above in various position relations and discovered the relation between geometry parameters and the characteristic of spectra
- Designed a model putting nanorod into cells for further calculation which can be utilized in cell imaging process such as SERS and fluorescence microscope based on its Fano spectra for signal enhancement

03/2016-04/2016 Cell classification and image processing, Advisor: Ishan Barman, Johns Hopkins University

- Utilization of cell profiler based on LOT method to find out the membrane of the cells in tissue
- Single cell is picked up using circling algorithm for classifying single cells for in cancer research
- SVM is utilized in the classification of single cells based on morphology patterns

04/2016-10/2016 Simulation of electrical enhancement and Fano resonance by Discrete Dipole Approximation, Advisor: Ishan Barman, Johns Hopkins University

- Established nanodisk structures on Solidworks with increasing height and fixed diameter on quartz substrate, extinction spectra and electric field on certain wavelength was calculated by DDA written in C++
- Determined the relation between Fano Dip and geometry parameters of the structure and wrote a manuscript based on the utilization of enhancing fluorescent absorption and emission based on the Fano Spectra characteristics

12/2014-06/2015 Research on the comfort of N95 filtering facial respirator by finite element analysis, Advisor: Hui Li, Wuhan University

- Converted headform CT model and FFR 3D model into CAD models through reverse engineering process followed by being meshed in Hypermesh for Finite element analysis
- Simulated the deformation of human headform during wearing process of FFR through LS-DYNA to acquire the distribution and intensity of pressure and to obtain the relation between pressure and Young's Modulus

03/2014-03/2015 Design and optimization of clinical nursing equipment based on clinical practice, Advisor: Zhuan Bian, Wuhan University

- Designed the structure in Solidworks and applied for Chinese Patent (ZL201410588536.X) for an automatic mouth gag for the post-operation restoration of cleft lip and palate patients
- Worked out the shape and acquired Chinese Patent for an alert mask (ZL201420695484.1) for cleft lip and palate infants
- Created the idea in Solidworks and obtained Chinese Patents (ZL201420762469.4, ZL201420774571.6) for high efficiency curing light and sterilization hat in clinical practice

PUBLICATION, PATENTS AND CONFERENCE

PATENTS:

- **Yaozheng Li,** Yan Mei, *A kind of prevention mask for cleft lip and palate patients*. ZL201420695484.1, 03/2015

- **Yaozheng Li,** Yan Mei, Wenjia Hu, *A kind of sanitizing cap for curing light in orthodontics.* ZL201420762469.4, 04/2015
- **Yaozheng Li,** Yan Mei, Wenjia Hu, *A kind of high efficiency curing light for orthodontics*. ZL201420774571.6, 04/2015
- **Yaozheng Li,** Yan Mei, *A kind of adjustable mouth open.* ZL201410588536.X, 04/2016

PUBLICATIONS:

- **Yaozheng Li**, Soumik Siddhanta, Ishan Barman. *Effect of substrate and height on gold nanodisk ensemble for plasmonic enhancement.* Applied Physics Letters. (Under Review)